Batteries & Supercaps

Research Article
doi.org/10.1002/batt.202400072

Chemistry Europe
European Chemical Societies Publishing

www.batteries-supercaps.org

Developing a High-Performing Spinel $LiMn_2O_4$ Cathode Material with Unique Morphology, Fast Cycling and Scaled Manufacture

Urbi Pal,[a] Binayak Roy,[b] Meisam Hasanpoor,[a] Hamid Ilbeygi,[a] Tiago Mendes,[a] Robert Kerr,[a] Lakshmi Vazhapully,[c] Chris Song,[c] Dabin Wang,[c] Matt Boot-Handford,[c] Mark G. Sceats,[c] Maria Forsyth,[a] Danah Al-Masri,*[a] and Patrick C. Howlett*[a]

High power application of Li-battery remains a challenge due to the lack of stable fast-charging cathode materials. Lithium manganese oxide (LMO) cathode is very promising due to its high operating voltage and fast charging ability; however, the associated Mn-dissolution is one of the main hindrances to its practical applicability. In this work, we demonstrate for the first time the use of a commercially scalable method through a proprietary Calix flash calcination (CFC) technology to develop high-performance electrode materials where a novel CXL LMO material was manufactured and tested. CXL LMO|Li metal cell showed a reversible specific capacity of 110 mAh/g with 99% retention after 100 cycles and showed excellent rate performance up to 20 C current rate (~20 mA/cm^2 current density). CXL LMO|Graphite cell (areal capacity 1 mAh/cm^2) was also reported with 86% capacity retention over more than 500 cycles. Cross-section morphology revealed a unique multi-layered structure that was retained at the core of the novel LMO material. It obtained lesser Mn dissolution compared to commercial LMO. The scalable synthesis procedure through CFC technology, can be broadly applicable to produce unique electrode morphology as demonstrated here for the CXL LMO representing a promising pathway for electrode manufacturing for high-power Li-batteries.

Introduction

The rapid electrification of electric vehicles (EVs) and ever-growing demand for high-power tools have motivated the search for diverse battery technologies. Modern-day commercial lithium-ion batteries (LIBs) extensively utilize cobalt-based cathodes, e.g., lithium cobalt oxide ($LiCoO_2$ or LCO),[1] nickel cobalt aluminum oxide (NCA), and nickel cobalt manganese oxide (NMC)[2,3] for various applications including portable electronic devices and electric vehicles. While these cathode systems provide high specific energy, their practical application is limited by a number of factors, such as their slower de-/lithiation kinetics and thermal runaway,[4] and also, their ethical sourcing.[5] In regards to thermal runaway, the exothermic degradation of LCO under overcharging conditions is one of the highest contributing factors to a Li-ion battery fire.[1] Mn-rich, lithium manganese oxides ($LiMn_2O_4$ or LMO) as cathode materials, on the other hand, provide several advantages over the other high energy layered–oxide materials, namely low cost, high operational voltage window (4.3 V) and a higher threshold against thermal runaway. Additionally, LMO does not suffer from overcharging and thermal runaway. The most promising advantage of LMO is its capability to support fast charging and discharging.[6] LMO has a cubic spinel crystal structure with an Fd3 m space group where the manganese ions alternate between close-packed oxygen planes, creating a 3D network of interconnected interstitial sites for lithium-ion transport.[7,8] This structure allows rapid lithiation/de-lithiation reactions that are required for high-power applications. These features make LMO systems very attractive for their intended applications including drones, power tools, heavy-duty transportation, and mining vehicles, where fast charging and/or discharging are desired. However, the utilization of the LMO cathode still faces challenges, mainly from the deterioration of capacity upon cycling at high voltage (> 4.3 V) at high rates. Capacity decay in LMO is believed to be caused by structural instability that originates from the irreversible phase transformation of spinel LMO, due to Jahn Teller distortion at the manganese (Mn) sites of the spinel framework and the subsequent dissolution of Mn^{2+} into the electrolyte. Various studies have reported that the dissolved Mn travels to the anode side and intercalates at the graphite anode, in LMO|graphite cells, resulting in a further decrease of Li de-/intercalation on the anode side and critical capacity loss.[9–11]

[a] U. Pal, M. Hasanpoor, H. Ilbeygi, T. Mendes, R. Kerr, M. Forsyth, D. Al-Masri, P. C. Howlett
Institute for Frontier Materials (IFM), Deakin University, Burwood, Victoria 3125, Australia,
E-mail: danah.almasri@deakin.edu.au
patrick.howlett@deakin.edu.au

[b] B. Roy
School of Chemistry, Monash University, Clayton, Victoria, 3800, Australia

[c] L. Vazhapully, C. Song, D. Wang, M. Boot-Handford, M. G. Sceats
Calix Limited, 71 Rowsley Station Road, Maddingley Victoria, 3340, Australia

Supporting information for this article is available on the WWW under https://doi.org/10.1002/batt.202400072

There have been many implemented strategies to synthesize LMO in the literature, the most common using stoichiometric amounts of $LiOH.H_2O$ and Λ-MnO_2 at 450–650 °C for 48–96 h.[12] The precursor of lithium sources has been reported to be varying from Li_2CO_3 to Li_3PO_4.[6] Various multivalent dopant cations were found to have a significant effect in limiting the Jahn–Teller distortion effect in LMO materials. Most recent examples include the doping effect of Mg,[13] Ti,[14] Cr,[15] etc., into the spinel lattice structure of LMO, which showed a significant increase in the performance of the cathode materials. Another approach included coating the LMO particles with a second composition to prolong their cycle life further. Examples include a coating of organic materials, e.g., polypyrrole,[16] poly (diallyldimethylammonium chloride),[17] conductive carbon,[18,19] as well as metal oxides, e.g., ZnO,[20] TiO_2,[21] Al_2O_3,[22] MgO;[23] these approaches are mostly aimed at limiting Mn dissolution, thereby hindering the phase change process discussed above.

Tuning the morphology to produce various nanostructures of the LMO particles was also found to play a significant role in improving high–rate discharge capacity and capacity retention. Solid state lithiation of porous Mn_2O_3 nanorods, prepared from the thermolysis of MnC_2O_4 powder, was reported to produce highly crystalline LMO nanorods, which enabled as high as 10 C cycling.[24] In another report, MnO_2 nanotube template and LiOH lithiation at a high temperature (700 °C) produced single–crystal LMO nanotubes, which showed long cycle life (1500 cycles) at a 5 C rate.[25] A hydrothermal lithiation technique of Mn_3O_4 was found to produce porous LMO nanowalls arrays which exhibited a high specific capacity of 131 mAh/g at 1 C rate with lithium titanium oxide (LTO) anode and the cell showed excellent rate capability of 97 mAh/g at 20 C rate.[26] Additionally, $LiMn_2O_4$ nanocubes with porous structure were found to effectively shorten the Li^+ transport paths, allowing $LiMn_2O_4$ material to realize excellent Li^+ extraction and insertion performance; the authors reported a discharge specific capacity of 95.39 mAh/g with a capacity retention rate of 90.91 % after 500 cycles.[27] Li et al. reported that a controlled growth of LMO particles could lead to the formation of a structure the authors refer to as the hierarchical porous onion with polyhedral crystal structure, which could efficiently suppress Mn dissolution.[9] These approaches are summarised in Table S1. Overall, the modification of Li diffusion pathways achieved by producing 'nanosized' LMO materials resulted in a longer cycle life than their larger aggregate counterparts. Despite these advances, the cost–effectiveness and purity requirements of these synthesis processes have still limited the broader application of spinel LMO materials. Additionally, the active material loading used to test the properties of these LMO materials has been limited to 1–2 mg/cm^2, below the values typically needed for practical applications. Therefore, the current literature is heavily focused on novel synthesis methods and producing unique LMO morphologies but lacks cycling performance with realistic active material loading as used with other high-performing commercial cathode chemistries (e.g. NMC, LFP, etc). Further, the synthesis methods reported to date are generally unscalable or scalable at a high cost, thus being unrealistic pathways for large-scale commercialisation and real-life application.

In this work, we report the synthesis of a novel LMO material by Calix Ltd. in a commercially upscaled process through a proprietary Calix flash calcination (CFC) technology. This technology produces a maximum 13 kg sample, upscaled from an initial 100 g batch, and the LMO produced using this technology is denoted as CXL LMO. The CXL LMO was prepared by an incipient wetness impregnation (IWI) method. Calix flash calcined high surface area manganese oxide (Mn_xO_y) and lithium hydroxide ($LiOH.H_2O$) solution were used as precursors. The CFC technology is able to flash calcine the precursor ($MnCO_3$) at a throughput of 100 kg/h to produce a high surface area Mn_xO_y (BET surface area is reported in supplementary Table 1) as an intermediate for subsequent LMO synthesis. A homogeneous particle distribution was achieved in this method at both small (100 g) and large–scale production (13 kg). The CXL LMO produced using the CFC method resulted in a unique multilayered structure. A practical active material loading of 7 mg/cm^2 was explored in this study which is significantly higher than the leading literature (1–2 mg/cm^2). Extensive electrochemical studies were carried out and the resulting CXL LMO materials were found to demonstrate stable cycling with 99% capacity retention at a 1 C rate and 70% capacity at an ultrafast cycling rate up to 20 C. These cathodes have a high areal capacity of 1 mAh/cm^2 which is higher than most of the literature where often low utilisation of cathode loading was reported.[26,28–31] The performance comparison is summarised in supplementary Table 2. Further, an Mn dissolution study was also performed, where the unique morphology of CXL LMO was found to reduce Mn dissolution compared to commercial LMO materials. Detailed characterization of the new CXL LMO materials including XRD, FIBSEM, ICPMS, and the electrochemical studies are reported in the following sections.

Results and Discussion

Structure and Morphology

Figure 1a shows the XRD pattern of the as-synthesised LMO, labelled as CXL LMO, where the powder pattern matches with the cubic $LiMn_2O_4$ structure with the Fd3m space group. Peaks around 45° and 65° have been assigned to the Al substrate (supplementary Figure S1). A similar pattern was observed for a commercial Shanshan LMO material (henceforth it is referred to as commercial LMO). Figure 1b shows the particle size distribution of both the LMO powders which was found to be within 10–100 μm, suggesting that both materials have similar particle distribution ratio. The SEM images (FESEM analysis) of the CXL LMO and commercial LMO are shown in Figures 1c and d, respectively, where the CXL LMO particles showed a unique multi-layered morphology. In contrast, the granular particle morphology of the commercial LMO is consistent with previously reported literature.[6] Debye–Scherrer analysis of the obtained diffraction data clearly shows a reduction in crystallite size, in particular along the '111' plane, typically correlated to the superior high rate cycling and stability performance of LMO electrodes. (Further characteristic information and discussion including the crystallite sizes, surface

Research Article
doi.org/10.1002/batt.202400072
Chemistry Europe
European Chemical Societies Publishing

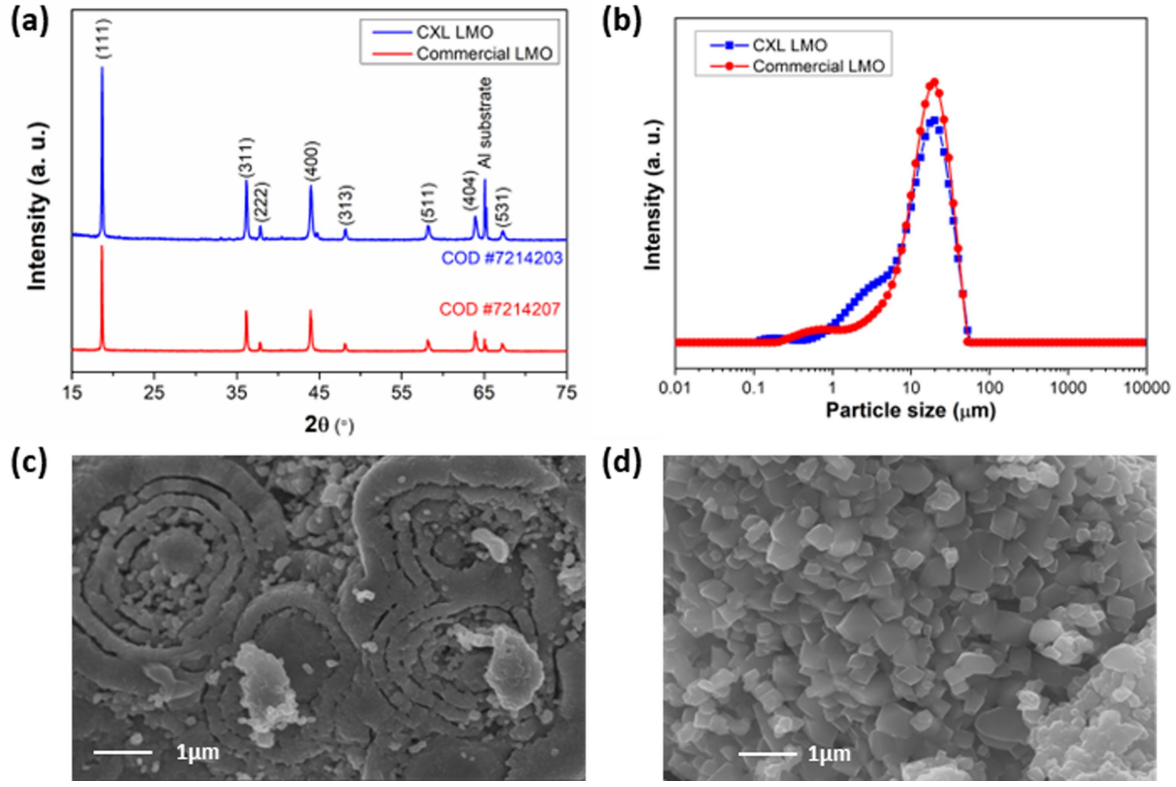

Figure 1. (a) XRD patterns of CXL LMO and commercial LMO where the patterns are matched against the crystallography open database (COD) number reported in each case. (b) Particle size distribution of LMOs. SEM images of (c) CXL LMO and (d) Commercial LMO powder.

area etc are mentioned in Supplementary Figure S1b and Table S1).

Electrochemical Study

Cyclic voltammetry (CV) was conducted to investigate the electrochemical performance of the newly synthesised CXL LMO. Figure 2a shows the cyclic voltammogram of the CXL LMO compared with commercial LMO (Figure 2b). Both LMOs showed two oxidation peaks at 4.06 V and 4.17 V followed by the reduction at 3.97 V and 4.09 V, which is consistent with the reported literature.[32] Importantly, the peak of CXL LMO showed a higher current and was a sharper peak compared to the commercial LMO. Continuous cycling of the CXL LMO material was conducted in a lithium metal cell to compare the capacity retention to the commercial LMO. The specific capacity obtained during cycling is shown in Figure 2c. The CXL LMO achieved a C/10 first discharge capacity of 110 mAh/g while the commercial LMO obtained a first discharge capacity of 120 mAh/g. After 1 C cycling for 60 cycles, a 70% capacity retention was achieved for the commercial LMO compared to 99% for the CXL LMO. The performance of CXL LMO is very promising as a 10 times increase in the current (from C/10 to 1 C) did not affect achieving the specific capacity of 110 mAh/g and its retention over cycling. The voltage profile in Figure 2d showed the commercial LMO developed higher overpotential over cycling from the 10th cycle to the 50th cycle, whereas CXL LMO showed no significant change in the voltage profile for the 10th and 50th cycles. It is also observed that the constant voltage charging step of the commercial LMO showed a larger contribution to the capacity compared to the CXL LMO. These behaviors are indicating faster Li kinetics for the CXL LMO electrode in the cell. Rapid capacity decay at longer cycles is attributed to the depletion of Li metal, typically observed with carbonate-based electrolytes[33] as reported in Supplementary Figure S2a.

The ability to sustain fast charge discharge is one of the main advantages of LMO cathode chemistry. In this work, fast discharge of the cathode was probed at current rates up to 20 C shown in Figure 3a, where superior performance of the CXL LMO is shown with no notable capacity decay up to 10 C with 93% capacity retention and then a moderate loss in capacity at 20 C with 77% capacity retention. The full capacity of the CXL LMO was recovered when the cells were then cycled at 1 C (note: here 1 C is equivalent to 1 mA/cm^2) after 90 cycles with 99% capacity retention, indicating the capacity loss is reversible and no permanent damage to the cathode material occurred. In comparison, commercial LMO showed a progressive decay in capacity in each step of the current rate increments and only 17% of capacity retention at 20 C, which was also recovered at subsequent 1 C cycling. The cycling voltage profiles from both the CXL LMO and commercial LMO cells are shown in Supplementary Figures S3a and S3b. While the behavior of both LMO electrodes is similar at lower C-rates, much higher polarisation is observed for the commercial LMO at higher rates, namely 4 C and 20 C. The voltage profile of the commercial LMO shows a longer constant voltage charging time at 4.3 V, indicating slower kinetics and growing

Research Article
doi.org/10.1002/batt.202400072
Chemistry Europe
European Chemical Societies Publishing

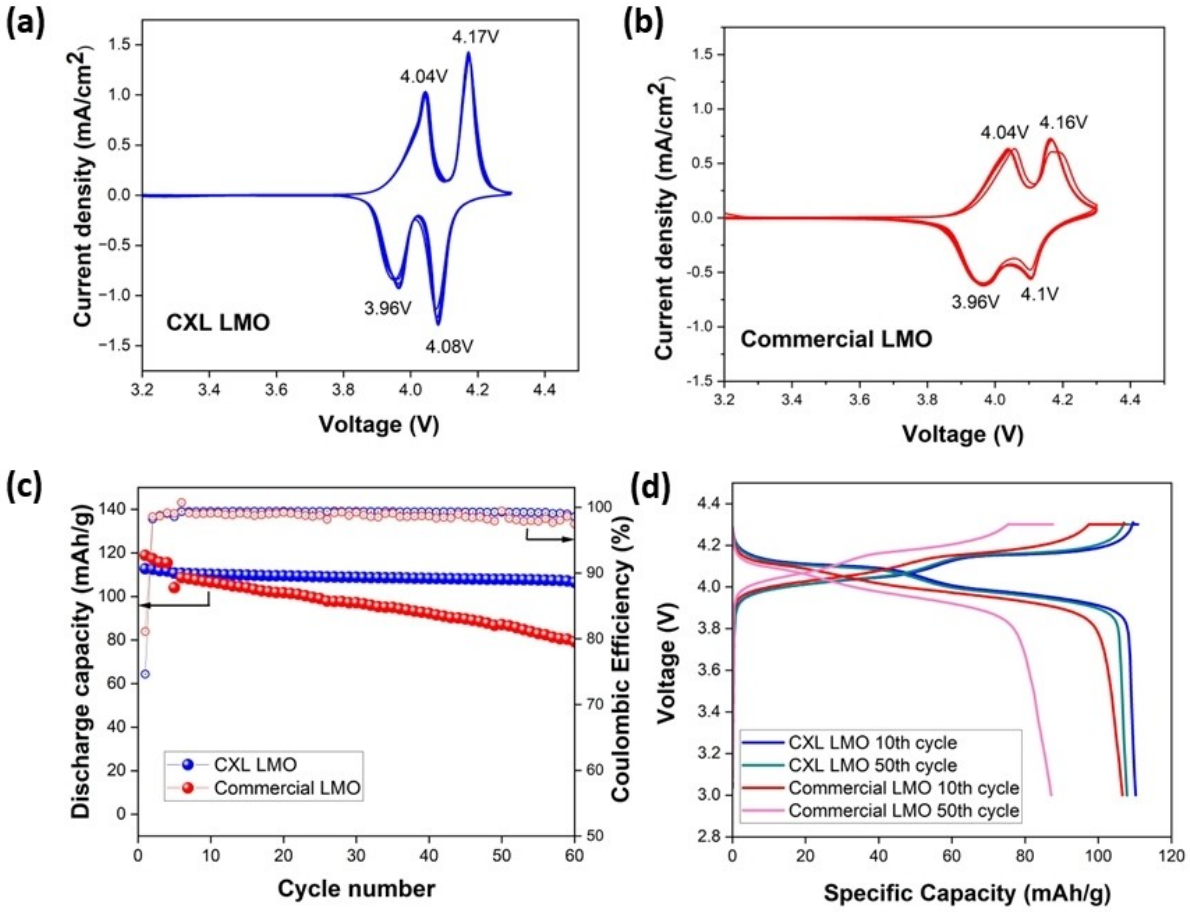

Figure 2. Cyclic voltammograms of (a) CXL LMO and (b) Commercial LMO at 0.05 mV/sec scan rate. (c) Long–term cycling of LMOs vs. Li (50 um) at 1 C rate. (d) Voltage profile of CXL LMO and commercial LMO at 10th and 50th cycle.

polarisation during the 1 C charging. In contrast, the CXL LMO showed a negligible increase in overpotential up to 4 C.

Extended cycling of a spinel cathode is likely to induce mechanical stress–related structural degradation which often manifests as cracks and fragmentation and compromises the electrochemical performance. To investigate this, the surface and cross-sectional morphology of the LMO electrodes was imaged both before and after cycling. The pristine electrodes are shown in Supplementary Figure S4, showing the unique multilayered morphology of the CXL LMO. The electrodes after cycling (cells from Figure 3a) confirm that the structural integrity of the cycled CXL LMO is maintained after 100 cycles at up to 20 C in Figure 3c. In contrast, the commercial LMO after 100 cycles under the same cycling conditions underwent significant cracking across multiple sites which can be seen in Figure 3d.

The most common drawback of LMO chemistry is considered to be manganese (Mn) dissolution during cycling. Here, ICP–MS was used for the comprehensive quantitative measurement of the dissolved Mn across the cathode, anode, and separator in both new CXL and commercial LMO systems after cycling for 100 cycles (cells from Figure 3a). The experimental procedure and Mn dissolution analysis are explained in detail in Supplementary Figures S5a and 5b, where both the Mn dissolution in electrolyte and Mn deposition on Li were found to be lower for CXL LMO (0.02±0.0022 wt% and 0.014±0.0028 wt%, respectively) than commercial LMO (0.3±0.0036 wt% and 0.02±0.002 wt%, respectively). This suggests that the superior cycling stability of CXL LMO is related to reduced Mn dissolution and that this is apparently a feature of the unique CXL morphology (Figure 3a & c).

The unique morphology of the CXL LMO particles apparently plays an important role in contributing to better cycling stability. As mentioned earlier, the voltage profiles of equivalent CXL LMO and Commercial LMO electrodes are shown in Figure S3 where CXL LMO shows a smaller overpotential at faster rates (4 C and 20 C) compared to the commercial LMO. The reduced overpotential in the case of the CXL LMO suggests faster Li^+ diffusion pathways through the interface of the unique structure, which allows the CXL LMO system to retain stability under high current rate cycling. Also, the better Li^+ diffusion across the interface of the CXL LMO cathode minimises its structural degradation (cracking) as well as Mn dissolution in comparison to its commercial counterpart (commercial LMO).

A comparative cycling performance study against LFP and NMC811 cathodes was conducted whereby a similar areal capacity of 1 mAh/cm^2 was used and their respective cycling performances are shown in Figure 3b. It can be seen that the NMC cathode fails to cycle at a high rate when it exceeds 3 C (3 mA/cm^2 of 1 mAh/cm^2) and results in cell failure. The NMC cathode performed the

Research Article
doi.org/10.1002/batt.202400072
Chemistry Europe
European Chemical Societies Publishing

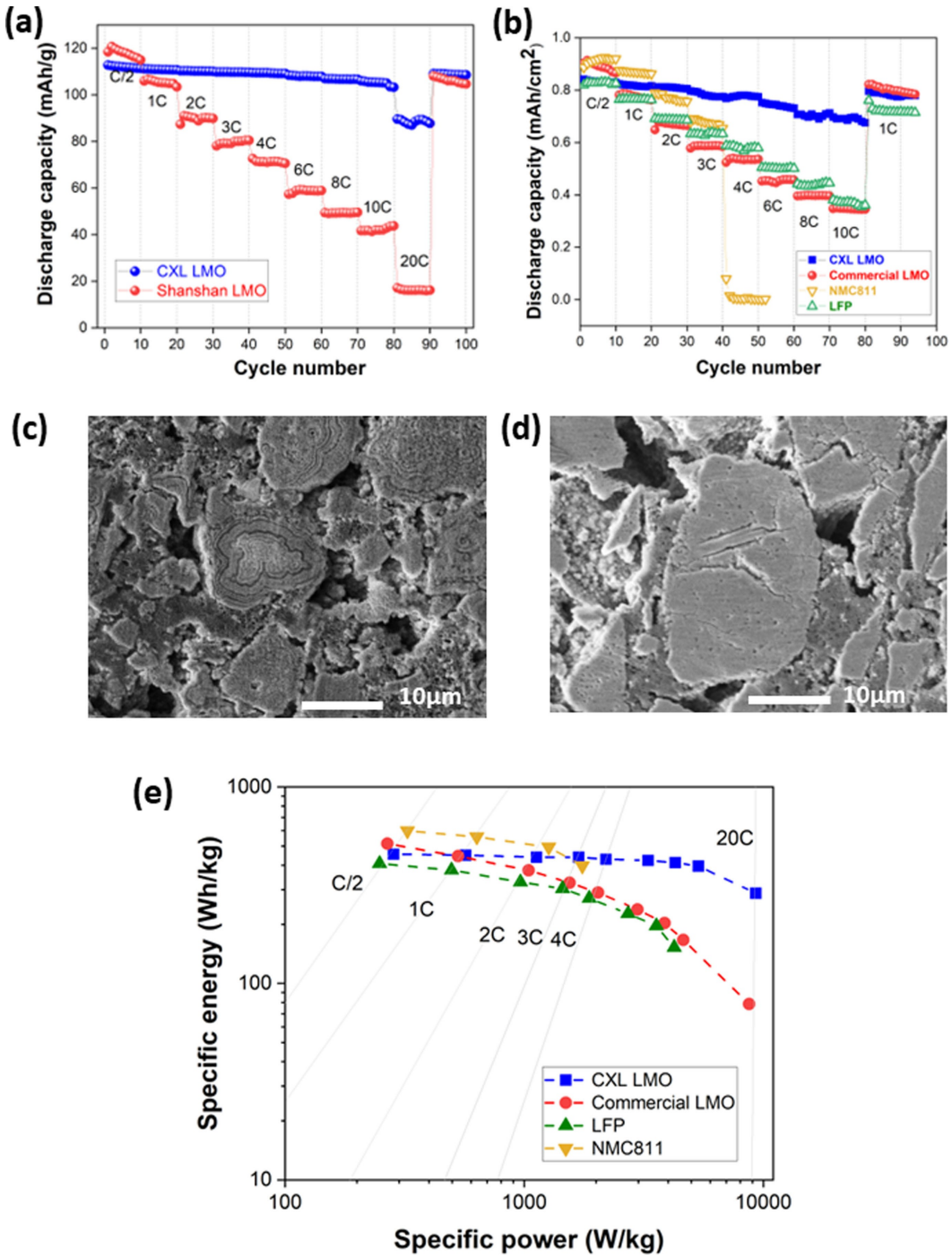

Figure 3. (a) Rate capability test with constant charging current at 1 C and different discharging currents from C/2 to 20 C and back to 1 C. (b) The rate capability of various cathodes using 1 mAh/cm^2 areal capacity cathode in a lithium metal full cell. Cross-sectional FIB–SEM images of (c) CXL LMO and (d) Commercial LMO electrodes after 100 cycles. (e) Specific energy vs specific power of various cathodes (active material loading of the cathode is considered for this calculation) assuming a lithium metal cell configuration. In all the experiments Li metal thickness was 100 um.

best at a slower rate of C/2 (0.5 mA/cm^2 of 1 mAh/cm^2). The LFP cathode could cycle throughout the cycling protocol and showed decreasing capacity similar to, or slightly better than, the commercial LMO. Importantly, the CXL LMO outperformed all other cathode chemistries and showed stable behavior throughout the experiment.

A Ragone plot in Figure 3e highlights the superior specific energy and specific power achieved for the CXL LMO compared to the cathodes studied in Figure 3d. It is seen that beyond a 4 C rate, the specific power drops rapidly for all electrodes except for the CXL LMO, which sustains its specific energy up to nearly 10,000 W/kg. This highlights the potential advantage of this electrode material for a range of high-powered applications from

Research Article
doi.org/10.1002/batt.202400072
Chemistry Europe
European Chemical Societies Publishing

drones to power tools. The performance comparison of various LMO systems from literature with the active material loading and other critical details are also tabulated in Supplementary Table 2. The CXL LMO material is superior in this class, despite having employed a higher cathode material loading of 7 mg/cm^2 in this study compared to the typically used value 1–2 mg/cm^2 in the literature.

Li-Ion Full-Cell Cycling

The comparative performance of Li-ion cells using the CXL LMO and commercial LMO cathodes coupled with a graphite anode is reported in Figure 4a. The initial coulombic efficiency (ICE) for the CXL LMO and commercial LMO cells were found to be 78% and 75%, respectively, which indicates the decrease in the first discharge capacity, believed to be due to solid electrolyte interphase (SEI) formation at the graphite anode.[34] To confirm that the low ICE is caused by SEI formation on the graphite anode,

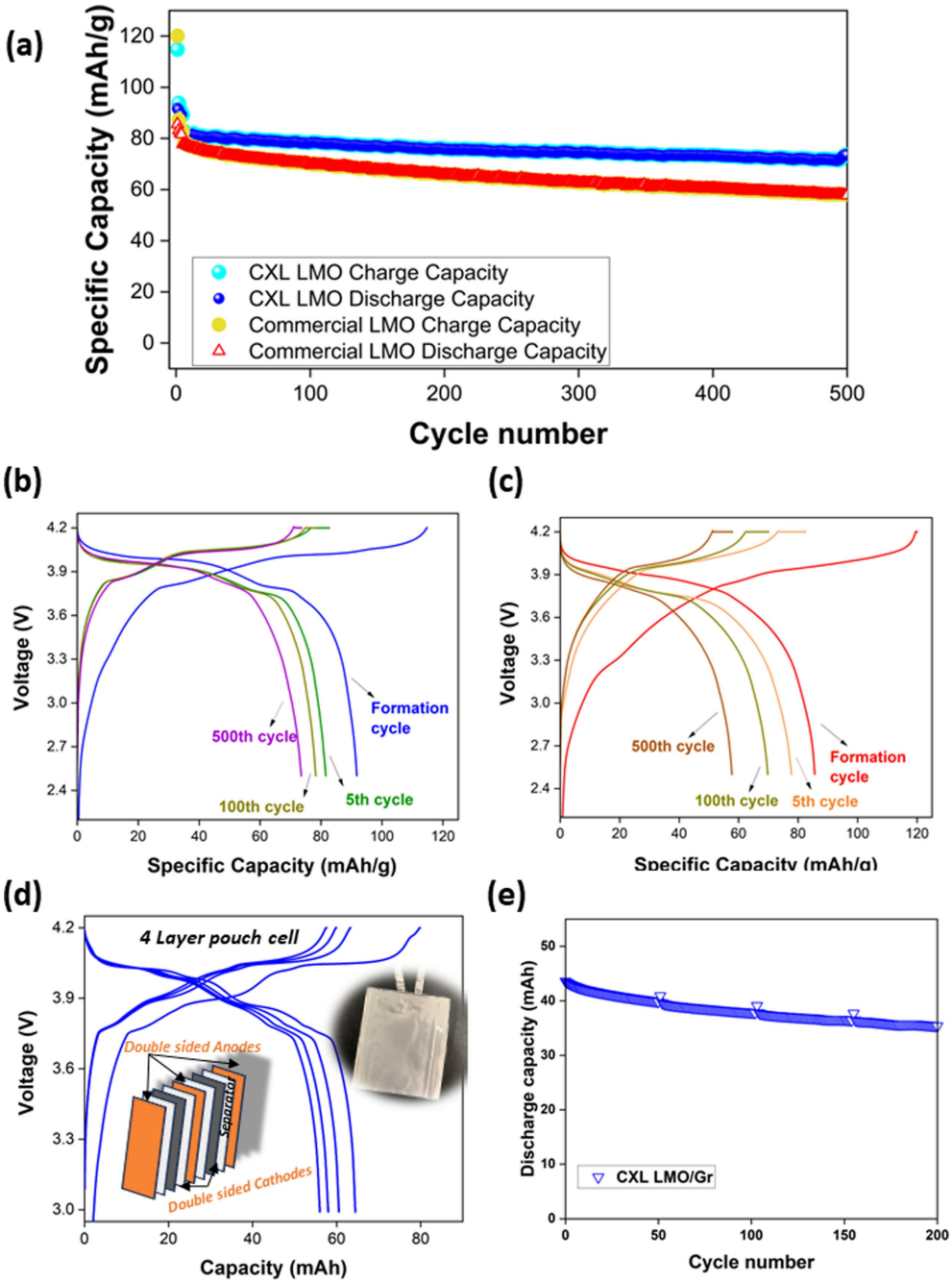

Figure 4. Full cell performance: (a) Long-term cycling of LMOs vs. Gr at 1 C charge-discharge rate (b) voltage profile of Li-ion cell of CXL LMO, and (c) commercial LMO, (d) the formation cycles of the 4 layer pouch cell made with 2 layers of CXL LMO double-sided coated cathode and 3 layers of graphite double-sided coated anode (e) long-term cycling of CXL | Gr cell at 1 C charge-4 C discharge for 200 cycles, a recovery step at C/10 current rate was set after each 50 cycles to facilitate the high rate long-term cycling.

Research Article
doi.org/10.1002/batt.202400072
Chemistry Europe
European Chemical Societies Publishing

a Li|Gr half-cell utilising the same electrolyte was tested (Supplementary Figure S6) and the ICE was found to be 78%. In Figure 4a, the Li-ion cells were cycled for 500 cycles at 1 C (1 mA/cm^2 of 1 mAh/cm^2) charge and discharge rate. Both LMO materials showed a steady capacity fade rate during cycling, with CXL LMO having superior capacity retention of 84% after 500 cycles (Figure 4b) compared with 73% for the commercial LMO (Figure 4c). This observation is consistent with the previous rate capability test (Figure 3a) as well as Li metal full cell cycling (Figure 2c), where the commercial LMO showed a faster capacity decay at 1 C compared to CXL LMO.

A four–layered pouch cell was assembled for purposes of demonstration using an electrode formulation, electrolyte ratio, and formation process that is not yet optimised. In Figure 4d, the cell demonstrated stable formation cycles at C/10 rate (where the nominal cell capacity is 55.8 mAh). Long-term cycling for 200 cycles of the four–layered pouch cell is also reported in Figure 4e where the charging rate was 1 C (55.8 mA) and a discharging rate of 4 C (223.2 mA) was applied. Such high current cycling resulted in very impressive performance with 81% capacity retention over 200 cycles. Thereby overall a stable cycling behavior of the upscaled material, sampled from a 100 kg batch (batch details are mentioned in the experimental section) and the preparation of double-sided coatings using 3 L slurry at the pilot scale, highlights the current status of the electrode scale–up.

Conclusions

A novel manufacturing route for the upscaled synthesis of lithium manganese oxide cathode material with a unique morphology and high surface area is reported. The new CXL LMO cathode showed ultra-stable performance at a 1 C rate with 99% capacity retention in a Li metal cell. A stable cycling performance and good capacity retention up to as high as 20 C rate (20 mA/cm^2 of 1 mAh/cm^2) was also reported. Throughout this manuscript, we have compared the performance of the new CXL LMO to commercially obtained LMO. Commercial LMO showed inferior capacity retention and faster capacity degradation, attributed to a higher degree of Mn dissolution and cracking of LMO particles during cycling. The performance of CXL LMO was also compared to NMC and LFP cathode chemistries and again showed superior performance in terms of capacity retention and long–term stability under the same cycling conditions with much improved specific power and specific energy. Demonstration of a 4-layer pouch cell was also reported, including formation steps and further detailed studies of pouch cell fabrication and testing is currently underway at our laboratories using the CXL LMO material. Additional materials characterisation is underway to understand the role of the CXL LMO morphology, phase change related to this material, and its relationship to the enhanced performance in more detail. Herein, the viability of preparing a high-performance, commercially relevant quantity of electrode material, exemplified here by the CXL LMO cathode active material, was demonstrated using the Calix Ltd upscaled manufacturing process.

Materials and Method

CXL LMO Preparation

Small scale (100 g): A Calix lithium manganese oxide ($LiMn_2O_4$ which is named CXL LMO) was prepared by the incipient wetness impregnation (IWI) method at lab-scale as a proof-of-concept to demonstrate the benefit of using high surface area precursor (Mn_xO_y) for $LiMn_2O_4$ synthesis. Calix flash calcined manganese oxide (Mn_xO_y) and lithium hydroxide ($LiOH.H_2O$) solution were used as precursors. To synthesize the material of interest, a saturated 0.5 M LiOH solution was first prepared by dissolving $LiOH.H_2O$ in de-ionized water using a magnetic stirrer at 30 °C. To synthesize $LiMn_2O_4$ via IWI, Calix calcined high specific surface area (HSSA) Mn_xO_y was dried and doped with saturated LiOH solution through multiple doping-drying cycles to achieve the target stoichiometry; The volume of solution in each cycle was calculated to be just sufficient to fill the pores of the powder to the incipient wetness point. The total volume of saturated LiOH solution added is fixed based on stoichiometry. As an example, 120 ml (or an appropriate amount) of saturated $LiOH.H_2O$ solution was slowly added in succession to 300 g of Mn_xO_y powder, with continuous mixing by mortar and pestle until Mn_xO_y powder fully adsorbed the liquid and formed a homogeneous mixture. The composite was then dried in a fan-forced oven at 100 °C for 48 hours. The above procedure was repeated until all the desired amount of LiOH solution was added. The resulting dried composite was ground using a motor and pestle and passed through a sieve with 100-micron mesh. 15 g of sieved precursors were placed in a ceramic crucible and lithiated at 800 °C for 2 h using a tube furnace with 1 L/min air purge via fast heating & cooling (i.e., the sample was put in once the furnace reached 800 °C and taken out after 2 h at 800 °C and stored in a desiccator at room temperature).

Large scale (13 kg): To avoid the time–consuming and labour–intensive processing with IWI method, a modified solution processing (SP) technique was used for Calix LMO synthesis at larger scales. Again, Calix flash calcined manganese oxide (Mn_xO_y) and saturated lithium hydroxide ($LiOH.H_2O$) solution were used as precursors. A dispersion of manganese oxide and saturated LiOH solution was prepared using a continuously stirred tank (CSTR) reactor. The mixture was heated under a vacuum at 120 °C for a few hours to reduce the water content, the resulting paste was transferred to porcelain trays and dried using a fan–forced oven at 100 °C for 72 h. The dried composite was ground using a ball mill and sieved. The precursors were placed in ceramic crucibles and lithiated at 800 °C for 2 h using a tube furnace with 1 L/min air purge via fast heating & cooling (i.e., the sample was put in once the furnace reached 800 °C and taken out after 2 h at 800 °C and stored in a desiccator at room temperature).

The CFC can flash calcine $MnCO_3$ precursor at a throughput of 100 kg/h to produce a high surface area Mn_xO_y. Mn_xO_y/LiOH is calcined to prepare the subsequent LMO synthesis which is currently at a max of around 13 kg per batch. The largest total of 100 kg batch of LMO is made up of calcination of multiple 13 kg batches of cathode active material precursor after sieving and particle size optimization. This large production of the batch is currently used in the pilot scale electrode coating. The performance of this batch is reported in Figure 4d.

Materials

CXL LMO cathode material was provided by Calix Ltd, an Industrial partner. Commercial LMO was obtained from Shanshan Corp. All the LMO powders were dried before making the cathode slurry. Carbon superP 65 was purchased from Sigma Aldrich and polyvinylidene fluoride (PVDF) was purchased from Alfa Aesar (99.9% purity). The graphite anode was purchased from Custom cells where the areal

loading of the anode material was 1.2 mAhcm^2. Separator Celgard 3501 was purchased from Hohsencorp and used as received. NMC 811 cathode was purchased from Customcells®, active material content 90% and active material mass loading 6.4 mg/cm^2, the areal capacity 1 mAh/cm^2. LFP cathode was purchased from Customcells®, active material content 90% and active material mass loading 6 mg/cm^2, the areal capacity 1 mAh/cm^2. The CXL LMO cathode was coated at lab scale with active mass loading ~7 mg/cm^2, active material content 90%, the areal capacity 1 mAh/cm^2. Li metal was obtained from LiFUN where the thickness was 100 um and stored in an Ar-filled glove box. LP30 electrolyte (composition of 1 M LiPF6 in EC/DMC) was purchased from Sigma Aldrich and kept inside the Ar–filled glove box.

Coin Cell Assembly

Cathode: Cathodes were prepared by drying the powder overnight. A ratio of 90% cathode material, 5% super C65, and 5% PVDF binder in NMP were dissolved and mixed using a speed mixer. The obtained mixture was coated on an Al foil and dried at 60 °C for 24 h in a fume hood. To dry off the solvent. The cathode film was dried further at 60 °C in a vacuum oven overnight before the electrochemical test each time. The same procedure is applied to various LMO materials, including CXL LMO, and commercial LMO.

A CR2032 coin cell was assembled for battery testing. Coin cell testing of LMO cathode foil with ~7 mg/cm^2 mass loading (an areal capacity of about 1 mAh/cm^2) was used for these studies. All the cathodes were cut into 8 mm diameter discs using an EL–Cell precision hand–held electrode cutter and dried before use. A lithium metal foil of 100 μm thickness (LiFun) (unless thickness mentioned otherwise) was used as the anode (and current collector) which was cut into 10 mm diameter for making the LMO|Li cells. Custom cell graphite anode was cut into 10 mm diameter and used in LMO|Gr full cells. Celgard 3501 was used as a separator and 45 uL LP30 electrolyte was used in each cell assembly in an Ar-filled glove box. The cathode-to-anode ratio of the full cell was 0.8 since the CXL LMO had an areal capacity of 1 mAh/cm^2 and graphite anode to be 1.2 mAh/cm^2.

The galvanostatic charge and discharge tests were conducted in the potential range of 3.0–4.3 V (vs. Li/Li$^+$) for the LMO|Li metal cell and 2.5 V–4.2 V for the LMO|Gr cell. All the experiments were conducted at 25 °C where the temperature was controlled in a Neware oven using a BCS cell test system (Biologic). The cyclic voltammetry (CV) test was carried out at a scan rate of 0.05 mV/s in the voltage range of 3.0–4.3 V. The long-term cycling of both LMO|Li and LMO|Gr cells were cycled at C/10 for 2 cycles (formation), then C/5 for 2 cycles, and 1 C rate thereafter. The charging was always at constant charge and constant voltage (CCCV) where the limiting current was applied to C/20 in each charging step. The discharge was carried out as a constant current discharge (CC) step. The rate capability test was carried out where charging was conducted at 1 C rate of constant charge constant voltage (CCCV) and constant current discharge at C/2, 1 C, 2 C, 3 C, 4 C, 6 C, 8 C, 10 C, and 20 C, each for 10 cycles and then back to 1 C. At least 3 replicate cells were conducted in each case. After cycling the rate capability tests the cells were kept for post-mortem analysis using FIB SEM and ICP MS test.

Pouch Cell Assembly

The CXL LMO (double-sided coating, areal loading per side 1 mAh/cm^2) cathode was cut to 31 mm×45 mm, and the graphite anode (double-sided coating, areal loading per side 1.2 mAh/cm^2) was cut to 32 mm×46 mm. All electrodes were dried under vacuum at 120 °C overnight prior to transferring to the glovebox. A 4-layer pouch cell was prepared by stacking the anode, cathode, and Celgard 3501 as separator (as per Figure 4d inset) and was assembled via bespoke robotic Z-stacker in an argon-filled glovebox. Ni and Al tabs were welded to the anode and cathode respectively. The LP30 electrolyte was used in an amount of 4.5 g/Ah. The final pouch cell is vacuum sealed using pouch vacuum sealing machine (MediaTech) and left to rest for 24 h at room temperature prior to the formation cycles. The entire process has been carried out inside the Ar filled glove box.

The galvanostatic charge and discharge tests were conducted in the potential range of 3 V–4.2 V for the LMO|Gr cell. The four-layer layer pouch cell has a nominal capacity of 55.8 mAh. The formation cycling was done at C/10 (5.58 mA) rate for 4 cycles followed by long term cycling. The cell was put for charging at CCCV at 1 C (55.8 mA) up to 4.2 V followed by CC discharge at 4 C (223.2 mA) until 3 V. A recovery step at C/10 rate was set at every 50 cycles to check the cell health and allow the high rate long term cycling. All the experiments were conducted at 25 °C where the temperature was controlled in a Neware oven using a BCS cell test system (Biologic).

Characterizations

XRD analysis was carried out using the powder sample of CXL LMO and commercial LMO. The XRD patterns were recorded using a Bruker D8 Advance X-ray diffractometer with Cu Kα radiation source (40 mA and 40 kV) within a 2θ range of 15°–75° with a 0.02° step and 0.5 s step-1. Electrode powders were placed on a flat, low background powder specimen holder and analyzed directly.

FIBSEM analysis was carried out for the cycled cells. The coin cells were disassembled inside an argon–filled glovebox using a coin cell disassembly unit (Hohsen). The cathode was dried under vacuum at room temperature for 15 minutes to evaporate the residual electrolyte before preparing SEM samples for imaging. To study the cross-section morphology and crack propagation in the cathode, the JSM-IT300 Scanning Electron Microscope from JEOL (Japan) was used with a 10 kV acceleration voltage. Additionally, the ion-milling instrument PECS 685 from Gatan was utilized to cut, polish the sample, and prepare the cross-section images.

ICP MS and Mn dissolution study was carried out for the cycled cells. The coin cell was opened by a coin cell decrimper and transferred to a 25×100 mm glass vial, followed by 2 ml DMC additionto the opened coin cell components. The LMO cathode and anode were separately collected and further washed with 0.5 ml of DMC. A total of 3 ml of the washed DMC liquid was treated as a stock solution. In a typical experiment, 30 μl of aliquot was collected and further diluted to 1.5 ml solution, which was used in the ICP–MS analysis. However, the dilution factor varied depending on the extent of Mn dissolution, so consistent results in ICP–MS analysis are received within 20–100 ppb concentration.

The DMC–washed Li anode foil was removed from the glove box in a sealed glass vial (under an Ar atmosphere) and placed in a dry ice bath. 10 ml mixture of ethanol, and 2% HNO_3 (5 ml:5 ml) were added to the Li metal dropwise, and the mixture was stirred until the effervescence ceased and the Li metal was completely dissolved. A schematic diagram is shown in Supplementary Figure S4. In a typical experiment, 1 ml of this aliquot was collected for further dilution by factors of ×10 times. However, the dilution factor has been varied to receive a consistent result from the ICP–MS analysis within 20–100 ppb concentration.

(Note: Treatment of Li metal under atmospheric conditions or the addition of water to Li **is highly exothermic and contains a flammability hazard**. This process aimed at mitigating the hazards by carrying out the reactions at very low temperatures and minimizing the exposure of metallic Li to the atmosphere. This process only applies to thin Li foils (50–380 μm) of 8–14 mm diameter, and not to a larger amount of Li).

Author Contributions

UP manuscript writing, experiment design and analysis, BR experiment design and analysis, MH FIBSEM analysis, HI pouch cell making, TM, RK experiment design, LV, DW and CS CXL LMO material synthesis and characterisation, MS and MBH lead the project, MF, DAM and PH intellectual contribution and project leadership. All authors contributed to manuscript preparation and reviewing.

Acknowledgements

This work is supported by the Cooperative Research Centres Projects (CRC–P) Grants where Calix Ltd was the industrial partner. This research was undertaken at the Deakin University Battery Research and Innovation Hub (BattRI-Hub), Australia. Professors Maria Forsyth and Patrick Howlett thank the ARC Industrial Transformation Training Centres StorEnergy fund. The authors acknowledge the FIBSEM facility, ICP–MS and XRD facility at Monash University and FESEM facility at Deakin University which were used to characterise the material in this work. The authors are truly grateful to Dr. Cuong Nguyen and Dr. Dijon Hoogeveen for XRD and ICP MS instrument operation. The facilities including BATMn flash calciner at Calix Ltd were acknowledged by the authors. Open Access publishing facilitated by Deakin University, as part of the Wiley - Deakin University agreement via the Council of Australian University Librarians.

Conflict of Interests

The authors declare no conflict of interest.

[1] L. Wang, B. Chen, J. Ma, G. Cui, L. Chen, *Chem. Soc. Rev.* **2018**, *47*(17), 6505–6602.
[2] M. D. Radin, S. Hy, M. Sina, C. Fang, H. Liu, J. Vinckeviciute, M. Zhang, M. S. Whittingham, Y. S. Meng, A. Van der Ven, *Adv. Energy Mater.* **2017**, *7*(20), 1602888.
[3] J. Kim, H. Lee, H. Cha, M. Yoon, M. Park, J. Cho, *Adv. Energy Mater.* **2018**, *8(6),* 1702028.
[4] A. W. Golubkov, D. Fuchs, J. Wagner, H. Wiltsche, C. Stangl, G. Fauler, G. Voitic, A. Thaler, V. Hacker, *RSC Adv.* **2014**, *4*(7), 3633–3642.
[5] L. Mancini, N. A. Eslava, M. Traverso, F. Mathieux, *Resour. Policy* **2021**, *71*, 102015.
[6] X. Tang, J. Zhou, M. Bai, W. Wu, S. Li, Y. Ma, *J. Mater. Chem. A* **2019**, *7*(21), 13364–13371.
[7] R. J. Gummow, D. C. L, M. M. Thackeray *Mater. Res. Bull.* **1993**, *28*, 1249–1256.
[8] M. M. Thackeray, P. J. Johnson, L. A. de Picciotto, P. G. Bruce, J. B. Goodenough, *Mater. Res. Bull.* **1984**, *19*(2), 179–187.
[9] Z. Li, X. Feng, L. Mi, J. Zheng, X. Chen, W. Chen, *Nano Res.* **2018**, *11*(8), 4038–4048.
[10] M. J. Lee, S. Lee, P. Oh, Y. Kim, J. Cho, *Nano Lett.* **2014**, *14*(2), 993–9.
[11] L. Jaber-Ansari, K. P. Puntambekar, S. Kim, M. Aykol, L. Luo, J. Wu, B. D. Myers, H. Iddir, J. T. Russell, S. J. Saldaña, R. Kumar, M. M. Thackeray, L. A. Curtiss, V. P. Dravid, C. Wolverton, M. C. Hersam, *Adv. Energy Mater.* **2015**, *5*(17), 1500646 .
[12] R. J. Gummow, A. de Kock, M. M. Thackeray, *Solid State Ionics* **1994**, *69*(1), 59–67.
[13] Y. Yu, J. Guo, M. Xiang, C. Su, X. Liu, H. Bai, W. Bai, K. Duan, *Sci. Rep.* **2019**, *9*(1), 16864.
[14] Y. Zhang, H. Xie, H. Jin, X. Li, Q. Zhang, Y. Li, K. Li, F. Luo, W. Li, C. Li, *ACS Omega* **2021**, *6*(33), 21304–21315.
[15] S. Q. Wen, L. C. Gao, J. L. Wang, L. Zhang, Z. C. Yang, S. K. Zhang, Y. L. Cui, *Key Eng. Mater.* **2014**, *636*, 49–53.
[16] T. Wang, W. Wang, D. Zhu, L. Huang, Y. Chen, *Mater. Res. Bull.* **2015**, *71*, 91–97.
[17] R. Vidu, P. Stroeve, *Ind. Eng. Chem. Res.* **2004**, *43*(13), 3314–3324.
[18] C. Jiang, Z. Tang, S. Deng, Y. Hong, S. Wang, Z. Zhang, *RSC Adv.* **2017**, *7*(7), 3746–3751.
[19] S. Lee, Y. Cho, H. K. Song, K. T. Lee, J. Cho, *Angew. Chem. Int. Ed. Engl.* **2012**, *51*(35), 8748–52.
[20] H. Liu, C. Cheng, Zongqiuhu, K. Zhang, *Mater. Chem. Phys.* **2007**, *101*(2–3), 276–279.
[21] C. Zhang, X. Liu, Q. Su, J. Wu, T. Huang, A. Yu, *ACS Sustainable Chem. Eng.* **2016**, *5*(1), 640–647.
[22] G. H. Waller, P. D. Brooke, B. H. Rainwater, S. Y. Lai, R. Hu, Y. Ding, F. M. Alamgir, K. H. Sandhage, M. L. Liu, *J. Power Sources* **2016**, *306*, 162–170.
[23] J. S. Gnanaraj, V. G. Pol, A. Gedanken, D. Aurbach, *Electrochem. Commun.* **2003**, *5*(11), 940–945.
[24] F. Cheng, H. Wang, Z. Zhu, Y. Wang, T. Zhang, Z. Tao, J. Chen, *Energy Environ. Sci.* **2011**, *4*(9), 3668–3675 .
[25] Y.-L. Ding, J. Xie, G.-S. Cao, T.-J. Zhu, H.-M. Yu, X.-B. Zhao, *Adv. Funct. Mater.* **2011**, *21*(2), 348–355.
[26] H. Xia, Q. Xia, B. Lin, J. Zhu, J. K. Seo, Y. S. Meng, *Nano Energy* **2016**, *22*, 475–482.
[27] H. Cheng, C. Ma, W. Li, *New J. Chem.* **2023**, *47*(11), 5244–5248.
[28] C. Xu, J. Li, X. Feng, J. Zhao, C. Tang, B. Ji, J. Hu, C. Cao, Y. Zhu, F. K. Butt, *Electrochim. Acta* **2020**, *358*, 136901 .
[29] D. K. Kim, P. Muralidharan, H. W. Lee, R. Ruffo, Y. Yang, C. K. Chan, H. Peng, R. A. Huggins, Y. Cui, *Nano Lett.* **2008**, *8*(11), 3948–52.
[30] H. B. Lin, J. N. Hu, H. B. Rong, Y. M. Zhang, S. W. Mai, L. D. Xing, M. Q. Xu, X. P. Li, W. S. Li, *J. Mater. Chem. A* **2014**, *2*(24), 9272–9279 .
[31] X. Xie, D. Su, B. Sun, J. Zhang, C. Wang, G. Wang, *Chemistry* **2014**, *20*(51), 17125–31.
[32] J. L. Wang, Z. H. Li, J. Yang, J. J. Tang, J. J. Yu, W. B. Nie, G. T. Lei, Q. Z. Xiao, *Electrochim. Acta* **2012**, *75*, 115–122.
[33] W. Xue, Z. Shi, M. Huang, S. Feng, C. Wang, F. Wang, J. Lopez, B. Qiao, G. Xu, W. Zhang, Y. Dong, R. Gao, Y. Shao-Horn, J. A. Johnson, J. Li, *Energy Environ. Sci.* **2020**, *13*(1), 212–220.
[34] J. Asenbauer, T. Eisenmann, M. Kuenzel, A. Kazzazi, Z. Chen, D. Bresser, *Sustain. Energy Fuels* **2020**, *4*(11), 5387–5416.

Manuscript received: February 1, 2024
Revised manuscript received: March 20, 2024
Accepted manuscript online: April 2, 2024
Version of record online: May 13, 2024